Final Report

Project Title:	Low-Cost III-V Photovoltaic Materials by Chloride Vapor Transport Deposition Using Safe Solid Precursors
Project Period:	6/15/16 – 10/31/17
Project Budget:	$225,000 + $56,486 cost share
Submission Date:	4/18/18
Recipient:	Shannon Boettcher, University of Oregon
Address:	Dept. Chemistry and Biochemistry 1253 University of Oregon Eugene, OR 97403
Award Number:	DE-EE0007361
Project Team:	University of Oregon, Lawrence Berkeley National Laboratory Molecular Foundry, Malachite Technologies Inc.
Contacts:	Shannon Boettcher Associate Professor, Chemistry Phone: 541-346-2543 Fax: 541-346-4643 Email: swb@uoregon.edu Shaul Aloni Staff Scientist Lawrence Berkeley Labs Phone: 510-486-7452 Email: saloni@lbl.gov Robert Weiss Malachite Technologies Phone: 415-307-4598 Email: rweiss@malachitetech.com

Executive Summary:

Si-based photovoltaic devices dominate the market. As photovoltaic (PV) manufacturing costs have plummeted, technologies which increase efficiency have become critical. Si cell efficiencies are nearing theoretical limits and Si-based PV modules are unlikely to reach the 25-30% efficiency range.[1] The use of III-V semiconductors is an obvious technical solution to improve efficiency, especially if they can be integrated directly with existing Si technology as tandems. High coefficients of light absorption along with tunable bandgaps and lattice constants have resulted in record conversion efficiencies for both one-sun and concentrator PV applications. GaAs, for example, has been used to manufacture single-junction photovoltaics with world-record efficiencies of 28.8% at one sun.[2] However, costs for III-Vs must be dramatically reduced to produce cost-effective, high-efficiency PV solutions.

III-V costs are controlled by two factors: semiconductor growth and the substrate. III-V growth is dominated today by metal-organic vapor phase epitaxy (MOVPE) with a lesser role played by molecular beam epitaxy (MBE). MOVPE costs are high due to the expense and low utilization (~30%) of precursors, modest growth rates (~100 nm min^{-1}), equipment complexity, and safety infrastructure needed to handle toxic, pyrophoric gases.[3] MBE costs are high due to slow growth rates and limitations of scalability. Details comparing plausible low-cost III-V growth methods are available in a review article published as a result of this project.[4]

The primary goal of this project was to demonstrate that close-spaced vapor transport (CSVT) using chloride (from HCl) as a transport agent can be used for the rapid growth of device-ready III-V layers from safe, solid-source precursors. In pursuit of this goal, we designed, built, and installed a new Cl-CSVT reactor based on insights from our previous H_2O-CSVT growth system and in collaboration with equipment professionals at Malachite Technologies. This system was successfully used to grow epitaxial GaAs with controlled *n*-type doping, having mobilities similar to MOVPE. Detailed technical information and results can also be found in the primary publication resulting from this project.[5]

This work sets the stage for tackling the development of high-performance III-V single junctions and tandem devices directly on Si substrates, which was beyond the capabilities of our H_2O-CSVT system. The design of the reactor's source and substrate transfer system should allow for direct deposition of device structures. The collective innovations of our Cl-CSVT system might ultimately serve as an enabling process for commercialization of the technology through a collaboration with appropriate industrial partners.

Table of Contents

Background:

Prior to the detailed discussion of the project outcomes in the area of CSVT deposition, we summarize the current commercialized technologies for III-V deposition as well as related low-cost technologies currently in the research stage in the context of the CSVT technology developed here.

Numerous growth methods have been developed over the past few decades to improve the quality of epitaxial III-V films or the cost-effectiveness of the growth method itself. The most prominent methods are metal-organic vapor phase epitaxy (MOVPE), molecular beam epitaxy (MBE), and hydride vapor phase epitaxy (HVPE) with less established methods also making headway (i.e. thin film vapor-liquid-solid (TF-VLS) growth and close-spaced vapor transport (CSVT)). Several reviews provide context for each of these methods along with their advantages and disadvantages.[4,6,7] Pertinent details relative to this project are highlighted below.

MOVPE and MBE: As mentioned earlier, MOVPE is still too expensive despite persistent use in commercial production. Recent economic analysis illustrates this methodology cannot support cost-effective production of III-V solar cells without radical changes.[8] The same is generally true of MBE, which is more cost prohibitive due to lower growth rates and scalability challenges of high-vacuum growth.[9] Both MBE and MOVPE had their start in the late 1960's[10] and have been extensively researched since the 1970's. This long history provides these techniques with a mass of collective knowledge, which competing techniques must catch up to. It does however, allow these techniques to serve as the benchmark for evaluating any material or device grown by alternative techniques.

HVPE: In this method, HCl reacts with a liquid group III metal at atmospheric pressure to generate the metal chloride species. Downstream, the group V hydride is introduced, forming a V-III-Cl complex on the substrate. Similar to MOVPE, gas phase dopants (e.g. silane, diethyl zinc) can be added to the mix. Through the addition of a pre-heating or second reaction zone more abrupt heterojunctions can be achieved. The Ptak group at the National Renewable Energy Lab (NREL) introduced both these designs.[11,12] Utilizing the two reaction zone design, they recently demonstrated an upright and inverted single-junction GaAs solar cell with a GaInP window layer.[13] The reactor design enabled the elimination of growth interruptions and both device geometries achieved conversion efficiencies above 20%. Our system design would also include a transfer mechanism, which aims to provide a path for more abrupt heterojunctions.

HVPE systems have also demonstrated capabilities to grow a variety of binary ternary, and quaternary III-V compounds. Recently, the NREL HVPE system demonstrated $In_{1-x}Ga_xAs_{1-y}P_y$ for top cell applications.[14] Similar to MOVPE, composition control of the group V elements is difficult compared to control of the group III elements, due to the high precursor input and differing rates of pyrolysis. Exploration of the growth parameters enabled growth of smooth films lattice matched to GaAs with $E_g \approx 1.7$ eV. Despite the strong performance in matching or exceeding aspects of MOVPE growth

there are still challenges for commercial application. The use of toxic arsine/phosphine, like in MOVPE, contributes to cost, along with the need for engineered gas flow. These associated systems costs could increase for a scaled system to meet commercial needs. The Cl-CSVT system, like its H_2O vapor predecessor, looks to expand on the use of solid precursors, eliminating the need for expensive gas precursors. Additionally, the CSVT system does not require engineered gas flows since the transport of gas species between solid precursor to substrate is diffusion limited. This has the potential to offer an alternative route to lower-cost devices utilizing the same materials investigated with HVPE.

TF-VLS: This technique provides more cost-effective devices by growing directly on low-cost substrates. The process was developed in 2013 by the Javey group. A layer of In metal is deposited on Mo foil and capped with SiO_x. The substrate is heated under H_2, with the introduction of a gaseous P source to facilitate growth. P diffuses through the SiO_x, becomes saturated, and reacts with the liquid In to nucleate InP. While this technique does not lend itself to easy heterojunction device growth, additional deposition of TiO_2 via atomic layer deposition or sputtering allowed the development and optimization of *p*-InP|*n*-TiO_2 solar cells.[15] The best device had J_{SC} = 26.9 mA cm^{-2}, V_{OC} = 692 mV, and *ff* = 65%, giving η = 12.1%; confirming the potential of this method for producing efficient, polycrystalline III-V PVs.

Further advances in the technique highlight its potential for III-V based polycrystalline PVs. Patterning of the metal substrate and In on a glass substrate afforded recent growths with effectively single-crystaline InP.[16] *In situ* doping with GeH_4 and preliminary growths of GaP and InSb were also performed. The possibility to grow effectively single-crystal III-Vs directly on amorphous surfaces could provide a very cost-effective route to virtual substrates. This is one advantage offered by this method the others cannot easily facilitate. While the method has some similarities to HVPE, the elimination of a single-crystal substrate and the subsequent device architectures are not as compatible with current state-of-the-art III-V devices. Other thin-film PV technologies like CIGS and CdTe may serve as a better benchmark for a TF-VLS grown InP device, where cells over 20% efficient have been shown.[2] Other VLS growths, such as GaAs nanowires demonstrated in HVPE[17] and MBE,[18,19] were used as a starting point for a similar demonstration in the Cl-CSVT system.

Cl-CSVT: Cl-CSVT looks to bridge the gap between the capabilities of HVPE and TF-VLS. Using all solid precursors with a targeted high precursor utilization, we leverage similar capabilities of TF-VLS to use low-cost starting materials. By using HCl as the transport agent, we generate equivalent (e.g. GaCl), or similar (e.g. As_2 vs. AsH_3), species as in HVPE, which gives us potential access to the same substrate and growth materials. CSVT is capable of selective-area growth, for possible use in nonplanar device architectures.[20] In principle, the use of HCl instead of H_2O will also allow growth on Si and could enable selective-area epitaxy of III-V nanowires for an alternative route to Si-based tandem cells.[21] The ability of CSVT to compete with MOVPE will be dependent on substantial work to demonstrate these capabilities, improved defect control, and greater breadth of III-V compounds. The beginnings of that demonstration come with the completion of this project.

Introduction:

Si-based PVs are a mature technology. With module costs below \$150 m^{-2}, total installed system costs are more-impacted by efficiency increases than by foreseeable reductions in areal cost. However, as Si cell efficiencies approach theoretical limits, Si PV modules are unlikely to reach above the 25-30% efficiency range.[1] Meanwhile, single-junction GaAs cells have already demonstrated record efficiencies of 28.8% at one sun.[2] Multi-junction III-Vs and mechanically stacked III-V tandems on Si both have record efficiencies greater than 31%.[2] Other III-V semiconductors, particularly GaAsP and GaInP, are appropriate band-gap materials to provide a stable, high-efficiency, top cell on Si. However, costs for III-Vs must be dramatically reduced to make these more efficient device architectures competitive with commercial Si PV.

III-V PV costs are controlled by two factors: semiconductor growth and the substrate. The dominant growth technologies, MBE and MOCVD, are much too expensive for widescale commercial production, as described in the background section. Single crystal substrates are prohibitively expensive, impeding the expansion of III-V solar technologies. New deposition methods need to investigate compatibility with inexpensive substrate technologies while also making deposition on existing single crystal substrates more cost-effective.

Here, we build upon the extensive research done with our Gen-1, H_2O-CSVT, reactor to further probe the capabilities of this deposition approach. We describe both undoped and *n*-type GaAs homoepitaxial growths with HCl as the transport agent in our Gen-2, Cl-CSVT, reactor. In addition to the properties of these films, we describe the reactor design itself and efforts to control defect formation.

CSVT was invented by Nicoll in 1963[22] and further developed by team members Prof. Boettcher and Dr. Aloni, who demonstrated potential to support low-cost III-V solar cell production. CSVT has limitations – such as its applicability to complex, low-dimensional structures – but it is well-suited to the simpler structures needed for solar cells. CSVT employs solid-source precursors, which become gaseous and are transported over short distances to grow at high rates (>1 μm/min). The reaction of the transport agent with the solid precursor for both the H_2O- and Cl-CSVT systems are shown in Equation 1 and Equation 2 respectively.

$$2GaAs(s) + 2H_2O(g) \leftrightarrow Ga_2O(g) + As_2(g) + H_2(g) \qquad \textbf{Equation 1}$$

$$2GaAs(s) + 2HCl(g) \leftrightarrow 2GaCl(g) + As_2(g) + H_2(g) \qquad \textbf{Equation 2}$$

This localized reaction, generating the volatile group III and V species, eliminates the need for pyrophoric, metal-organic and toxic, hydride species. The reaction is fully reversible and thus materials utilization can approach 100%.[22] Other transport agents include HCl and I_2; however, these have not previously been explored or discussed in great detail.[23]

Prior to this work on Cl-CSVT, there had not been any attempt to design a CSVT reactor capable of scaling to substrate sizes larger than ~1 cm^2. Additionally, there is only one prior instance of GaAs epitaxy via CSVT with HCl as the transport agent.[24] In that instance, GaAs was deposited onto GaAs and Ge substrates with emphasis on the later.

However, there is limited characterization of the as-deposited GaAs layers and process parameters such as temperature gradient were not explored in detail. HCl and similar hydrides or halides are used in other vapor transport methods (e.g. HVPE) to successfully execute thin film deposition. To realize the potential of Cl-CSVT to fulfill the need for a more cost-effective III-V deposition method, the full deposition system must be re-envisioned and investigated. To accomplish this a new system, which is compatible with the use of HCl, capable of growths on larger substrates to demonstrate feasibility, and reduces or eliminates other functional and engineering designs that hindered previous systems is described. This work is the necessary stepping stone to further evaluate the merits of this deposition method for cost-effective solar cell production.

Summary of Statement of Project Objectives and Milestones

Task 1.0: Design, Build and Delivery of Chloride CSVT system

Subtask 1.1 Finalize system requirements.

Milestone: System definition document will be completed.

Through coordination with, and contributions from, each of the three project teams (Prof. Boettcher, Dr. Shaul Aloni, and Malachite Technologies Inc. staff) we established a document which defined process control requirements (gas flow, temperature range, pressure range) as well as hardware configuration requirements (substrate size, sample exchange strategy, system scalability). This served as the foundation for all design considerations for the Gen-2 Cl-CSVT reactor.

Subtask 1.2 Engineering of Cl-CSVT system.

Milestone: Completed design phase and materials/components specifications with detailed Bill of Materials. System design will be in 3D design software (e.g. SolidWorks).

Cl-CSVT system was designed and engineered with frequent interaction between project teams. System was determined to meet the system definition document under Milestone 1.1. 3D part designs and Bill of Materials shared in online depository.

Subtask 1.3 Procurement and build of system.

Milestone: Cl-CSVT station installed at the UO and UO graduate students trained in safety aspects, maintenance and operation of the station.

Cl-CSVT system was installed at the UO lab. Collaborators from Malachite worked with graduate students to install system and train in safety, maintenance, and operation aspects of system. System successfully loaded and transferred substrates and was capable of running process recipes defined by UO personnel.

Task 2.0: Hardware and Process Development in Cl-CSVT Systems

Subtask 2.1 Growth of GaAs layers with “MOCVD-equivalent” materials properties in the Cl-CSVT system.

Milestone 2.1: Epitaxial *n*-type GaAs films with carrier concentration between 10^{17} and 10^{18} cm^{-3} and electron mobility > 2500 cm^2 V^{-1} s^{-1} will be demonstrated. Epitaxial

growth will be confirmed by high resolution x-ray diffraction. Mobility data will be verified by Hall effect measurement.

We demonstrated that *n*-type doping can be achieved using an *n*-type GaAs source wafer. A source wafer with Te dopant concentration of $1.96x10^{18} \pm 0.32$ cm^{-3} was used. An intentionally doped film using this source had a carrier concentration of $4.07x10^{18} \pm 1.42x10^{18}$ cm^{-3}, which suggests near unity utilization of Te. Initial electron mobilities were between 1050 and 1500 cm^2 V^{-1} s^{-1}. SIMS measurements indicated the low mobility was influenced by unintentional sulfur impurities coming from the uncoated graphite carriers. Use of pyrolytic coated graphite significantly reduced the sulfur content and resulted in an undoped electron mobility as high as 2156 cm^2 V^{-1} s^{-1}. Growth rates of ~ 0.1 to 0.3 µm/min were achieved between substrate temperatures of 700 to 800 °C respectively. Growths were confirmed to be epitaxial with high resolution x-ray diffraction (XRD). Source utilization was measured by both weighing source and substrate before/after growth in addition to mass calculations via film growth volume determined from optical profilometry measurements.

Subtask 2.2 Growth of AlGaAs window layer.

Milestone 2.2: $Al_xGa_{1-x}As$ films with *x* between 0.3 and 0.7 grown epitaxially on GaAs with thickness between 10-100 nm will be demonstrated.

Milestone 2.3: Demonstrate $Al_xGa_{1-x}As$ (x ~ 0.4) passivation of GaAs that results in PL lifetimes that are at least 50% as long as those of the MOVPE AlGaAs/GaAs/AlGaAs control samples, which are known to have low surface recombination velocities (~10^2 cm/s).

Neither of the above milestones under subtask 2.2 were achieved. Initial delays in the build and installation of the Cl-CSVT system along with additional process troubleshooting did not allow for enough time to begin growths of AlGaAs material.

Project Results and Discussion:

As outlined in the statement of project objectives summary above, the project consisted of two main tasks, which aimed to (1) design, build, and install a novel Cl-CSVT reactor at UO and (2) begin evaluating deposition method capabilities by demonstrating successful *n*-type doping of GaAs films and growth of AlGaAs films with growth and material properties comparable to HVPE and MOVPE. These two elements are the necessary first stages to effectively evaluate this deposition method as a viable alternative for a low-cost top cell, and possible integration with a Si bottom cell.

Task 1.0: Design, Build and Delivery of Chloride CSVT system

Finalize system requirements (Subtask 1.1)

Through various communications between all collaborators we established a system definition document, which served as the reference point for design specifications of the Cl-CSVT system. The document included process control requirements (gas flow, temperature range, pressure range) as well as hardware configuration requirements (substrate size, sample exchange strategy, system scalability). The specifics of these requirements are not listed here in detail, however crucial elements are highlighted in the subsequent engineering and installation subtask descriptions.

Engineering of Cl-CSVT system (Subtask 1.2)

We have utilized a simple, designed in house, reactor for previous work on H_2O-CSVT.[25] While functional, there are a number of features identified for modification in the design of a more robust reactor for use with Cl-CSVT. These include (i) material selection and corrosion resistance, (ii) independent component motion and control, and (iii) isolation of components from sources of contamination. Details of the old reactor are not discussed further but the design considerations themselves are touched upon in the following sections.

Material selection was crucial to minimize the potential for unwanted dopants or contaminants from corrosion and etching, which has been observed in similar systems.[26–28] Designing a reactor with numerous moving parts, the ability to independently move source and substrate samples, and enabling scalability required a larger chamber than would be feasible for quartz tubing used for the H_2O-CSVT system. Additionally, fused quartz is known to react with HCl at high temperature to generate Si impurities.[29,30] Alternatively, graphite has a high chemical resistance to HCl.[31–33] While numerous metal alloys will corrode, to varying degrees, in the presence of HCl,[33–35] 316L is the most corrosion resistant of the common, commercially available stainless steel alloy grades.[34,36] Therefore, carbon and 316L stainless steel were selected as the two primary components (see Figure 1). All components in contact with, and immediately surrounding, the source and substrate are made of pyrolytic coated graphite.

To minimize the potential corrosion of the stainless steel it is important to keep it below 200 C.[33,34] In order to control the temperature of the stainless components the chamber body and baseplate are double-jacketed for water cooling. This enables greater control of the chamber surface temperatures and helps isolate the growth zone as the only place where etching or deposition occurs.

Carbon was selected for the heating element itself. Here, a carbon-carbon composite is used for its structural stability, thermal and electrical properties, as well as machinability.[37] The thickness and element pattern were optimized for our power supply to deliver adequate heating. Oxidation of graphite is a problem at our deposition temperatures (750-850 °C), but this can be avoided with process controls and enclosing the composite heaters in pyrolytic graphite. Both the source and substrate heaters are independently controlled and monitored with thermocouples (TCs).

The source and substrate carriers were made of graphite. This enables custom machining of those parts to control additional process variables such as the spacing distance between source and substrate, which is fundamental to the CSVT growth process.[38] To minimize cross-contamination dedicated source carriers can be used for different III-V compositions or dopants. The use of pyrolytically-coated graphite serves to eliminate outgassing as well, which is discussed later.

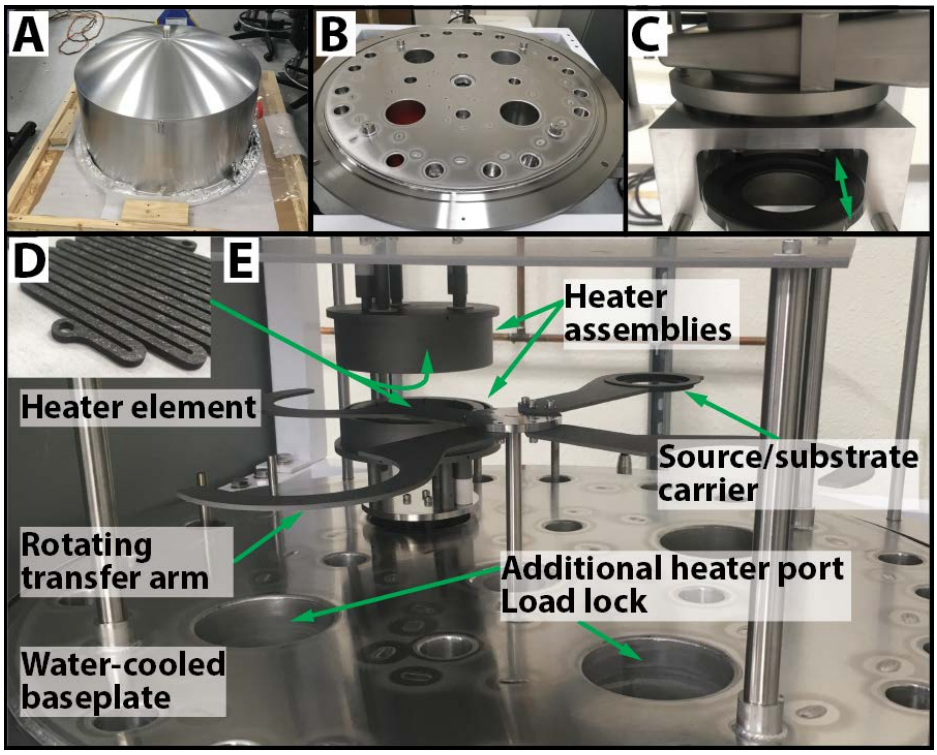

Figure 1: Images of individual, and assembled, components for the Cl-CSVT system. (a) Double-jacketed chamber dome, which encapsulates the whole system. (b) The water-cooled baseplate. Transfer from load lock and feedthroughs for heater assembly pass through pre-machined ports. (c) Load lock with pull out drawer (green arrow) for manual transfer of substrate carrier. (d) Four-inch carbon composite heating element. There is one in each of the heater assemblies. (e) Overview of internal assembly components. Rotating transfer arm brings the source carrier to the heater assembly and substrate carrier between there and the load lock.

The transfer of source and substrate carriers are executed independently from each other (Figure 2). A rotating arm assembly can pick up the two unique graphite parts for transfer to/from the reactor and the growth zone. Similar to the Ptak group's two-stage HVPE reactor, the design of the Cl-CSVT reactor included the capability to house multiple source materials for sequential homo- or heteroepitaxial growths with any necessary doping as well. Since the bottom heater moves up and down to allow the loading and unloading of the graphite carriers, it has flexible electrical contacts to minimize stress on those components if they were to become embrittled. Other electrical contacts are made via graphite itself or metal contacts housed inside of graphite components to minimize possible reaction with process gas. To minimize exposure of the source or substrate to atmosphere a load lock was also installed. With the sample transfer arm this enables the removal and insertion of substrate independent of any source carrier transfer. By eliminating the need to physically secure the source and substrate components together, as in the H_2O-CSVT, we enable substrate loading/unloading without exposing the source to atmosphere.

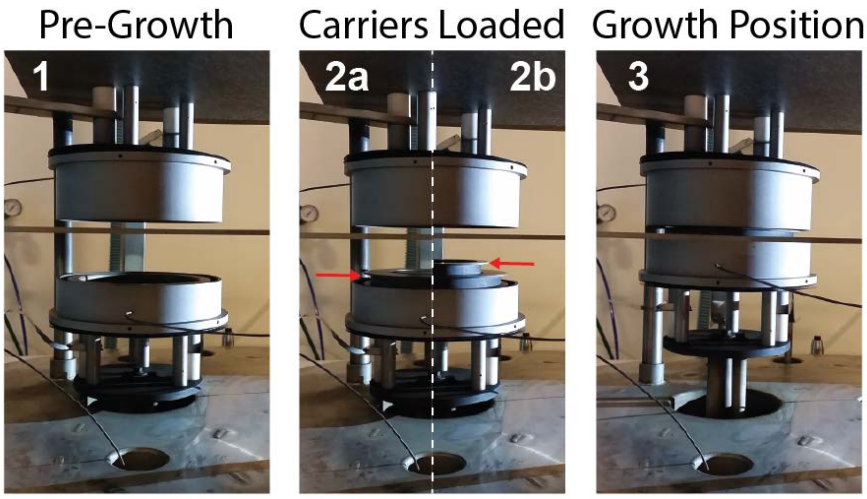

Figure 2: Source and substrate transfer process at growth zone. Prior to loading heater assembly is empty. Source carrier is loaded above bottom heater, followed by the substrate carrier on top of that. Prior to growth bottom heater assembly is raised to bring substrate carrier closer to top heater assembly.

The system controls were also designed to try and maximize modularity and simplicity. All components are housed inside an electrical panel for easy access. Safety circuits, circuit breakers, and other general power connections are housed in the top of the panel. Power supplies for the individual chamber components (valves, motors, etc.) are housed in the middle section. The programable logic controller (PLC) is a set of modular components from MKS. This enables communication from our computer, which is controlled with a LabView program, to the reactor. These modules relay the necessary controls to the individual chamber components. This allows for easy addition of additional components (i.e. TCs, gauges, etc.) or modules themselves in the future if further capabilities are needed. The LabView control on the user end also enables us to readily edit the program to meet various recipe or process parameter needs in the future.

Procurement and build of system (Subtask 1.3)

This system prototype, professionally designed by collaborators at Malachite Technologies and installed at UO, is the first major component of the final deliverable. The design considerations were the collection of first-hand knowledge from the current CSVT system at UO and the industry experience of the Malachite staff. Both teams emphasized the first-time right design of the system to minimize future challenges with regard to overall design and functionality.

System installation was completed in mid-February 2017. As built, the system is capable of supporting growth between pressures of 1 and 700 torr, with full motion of the bottom heater above 400 torr. The graphite carriers for source and substrate can be machined to accommodate different sample sizes (up to 2 inch wafers) and different spacer heights for the close-spaced reaction zone. The substrates can be loaded/unloaded into the process chamber through a load lock, minimizing atmospheric exposure of the other growth zone components including the source material.

Computer controls enable quick and accurate movement of source, substrate, and heating elements. Temperatures up to 900 °C have been achieved within the system under nitrogen and hydrogen environments. Process gas introduction is controlled via mass flow controllers and cannot exceed a pressure of 700 torr, to ensure system is not over pressurized with process gas under operation. The heaters themselves cannot operate unless the system's water cooling is also on, ensuring chamber components do not reach temperatures where sufficient corrosion could cause contamination.

The design of the chamber itself provides future scalability for the system. As seen in Figure 1, the heater assembly does not occupy most of the space inside the chamber. There are four ports in the base plate; one is for the load lock, and one for the existing heater assembly. The two remaining ports would enable the addition of two more heater assemblies, enabling simultaneous growths or growth zones dedicated to certain film types to minimize cross-contamination. While not trivial, the ability to add additional heater assemblies to the chamber with minimal modifications or other added parts is a testament to the forethought put into this design. In this regard, it is a significant improvement upon the original proposal, where additional chambers and gate valves would need to be added on, greatly adding to the cost and size of the system. Here, we have a one-size fits all chamber that will execute the short-term and long-term goals of this research group. Thorough design of the system allowed for rapid installation and successful safety checks. This enabled the group's work to focus solely on investigating the growth parameters necessary for high-quality films without additional time needed for equipment troubleshooting.

Task 2.0: Hardware and Process Development in Cl-CSVT Systems

Growth of GaAs layers with "MOCVD-equivalent" materials properties (Subtask 2.1)

We have investigated numerous process parameters to identify conditions necessary for repeatable, high-quality films. While the overall growth process is similar to the H_2O-CSVT system our group is familiar with, the different chemistry and reactor configuration precluded us from repeating previous process parameters and achieving the same growth results. Due to the differences in several conditions/parameters this prolonged the efforts to achieve Subtask 2.1. This included the unintentional presence of oxygen and sulfur, the temperature gradient and subsequent growth rates, surface features, and orientation dependence on growth. The investigation into these details and experimental methods to enable completion are highlighted in the following sections.

Growth Rate and Materials Consumption:

Real Temperature Gradient

Based on the H_2O-CSVT system, and similar HCl vapor systems, we were targeting growth rates on the order of ≥ 0.1 μm min^{-1}, ideally near 1 μm min^{-1}. Initially, growth rates were slower by roughly an order of magnitude. This turned out to be due to a discrepancy between the heater setpoint temperature and the local source/substrate temperature. Similar discrepancies have been noted in previous publications.[23,38] This led to an investigation to obtain a more accurate picture of the actual temperature gradient between source and substrate. Utilizing the machinability of our prototype graphite carriers, a hole was drilled into each for TC placement to correspond with the approximate position of

source and substrate wafers. The difference between our operating condition and this test condition are highlighted in Figure 3A. Currently, there are only two TCs in the reactor, which control the two heaters. To make repeatable measurements with the same TCs in different positions we operated the system with several constant heater power setpoints. Repeating this process with the TCs in both positions established a correlation between the two positions (Figure 3B). This would also enable the calculation of a temperature gradient under similar temperature setpoints that were not explicitly tested in this experiment. In general, the local temperature gradient between source and substrate was smaller by roughly a factor of 4 compared to the heater TC gradient being measured.

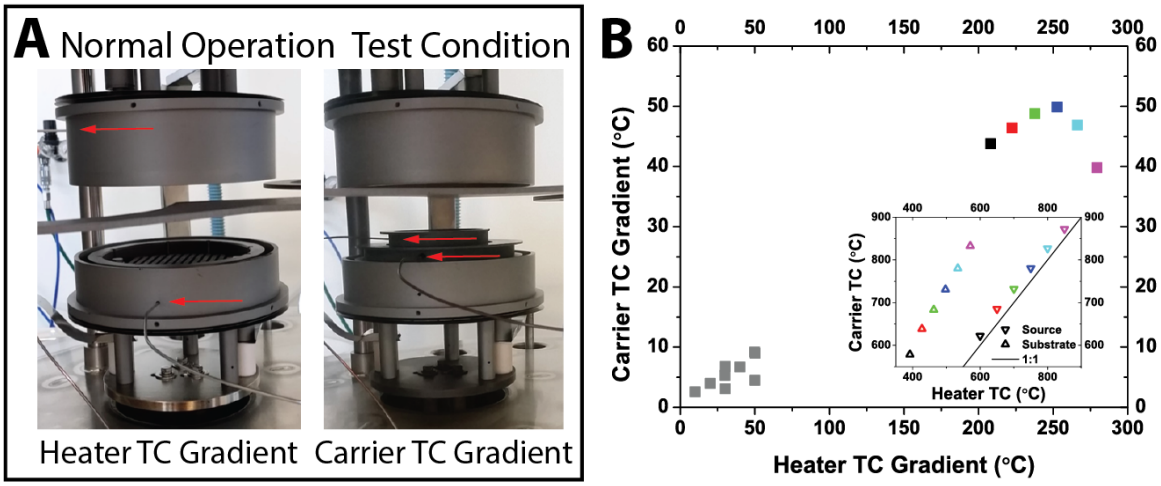

Figure 3: Temperature measurement positions and real temperature gradient measurements. (a) Image showing the placement of TCs for measurements made in (b). Gradient label on bottom of each position corresponds to the axis on plot. (b) Plot of gradients between source and substrate carrier compared to gradient reported by heater TC locations. Achieved gradient is roughly a factor of 4 smaller than reported from TC operating condition. Inset shows the correlation of source or substrate carrier with the bottom or top heater respectively. Colors correspond to the gradient plot. At these larger carrier TC gradients, >40 °C, the substrate is roughly 200 °C hotter than reported by the top heater TC. This currently limits the maximum achievable gradient between source and substrate carrier to roughly 50°C.

Growth Rate

With a more accurate understanding of the local temperature gradient between source and substrate the growth rate at several temperatures and temperature gradients was determined. The highest growth rates where achieved with increasing temperature and increased temperature gradient. A maximum source-to-substrate gradient of approximately 50 °C was achieved in this system. Growths with a similar gradient at a substrate temperature of ~800 °C had growth rates as high as 0.3 µm min^{-1}.

Transport efficiency

The transport efficiency of this growth method was also investigated. Utilization of the group III and V precursors in MOVPE is around 30 and 20% respectively.[4] While the utilization for CSVT growth is 100% in principle, the design cannot always ensure a completely closed system. Measurements of source and substrate films pre- and post-growth, in addition to a mass calculation from the volume as measured via optical

profilometry, indicated utilization as high as 64%. It is expected that further improvements could be made with additional engineering designs for the source and substrate carriers.

Doping:

Presence of Oxygen and Sulfur

The initial run on the system resulted in the formation of a gallium oxide, which was confirmed via energy dispersive spectroscopy (EDS), shown in Figure 4A. However, subsequent growths have shown stoichiometric GaAs without the presence of a surface oxide (Figure 4B). The source of the oxygen is believed to have been adsorbed oxygen in the porous graphite and the stainless steel body of the reactor itself. The collective surface area of this reactor is significantly greater than our Gen-1 reactor so it is reasonable to expect that additional thermal and vacuum treatment is needed to bring any adsorbed oxygen concentration to acceptable levels. While no oxide films have been seen since the initial growth, several measurements with time-of-flight secondary-ion

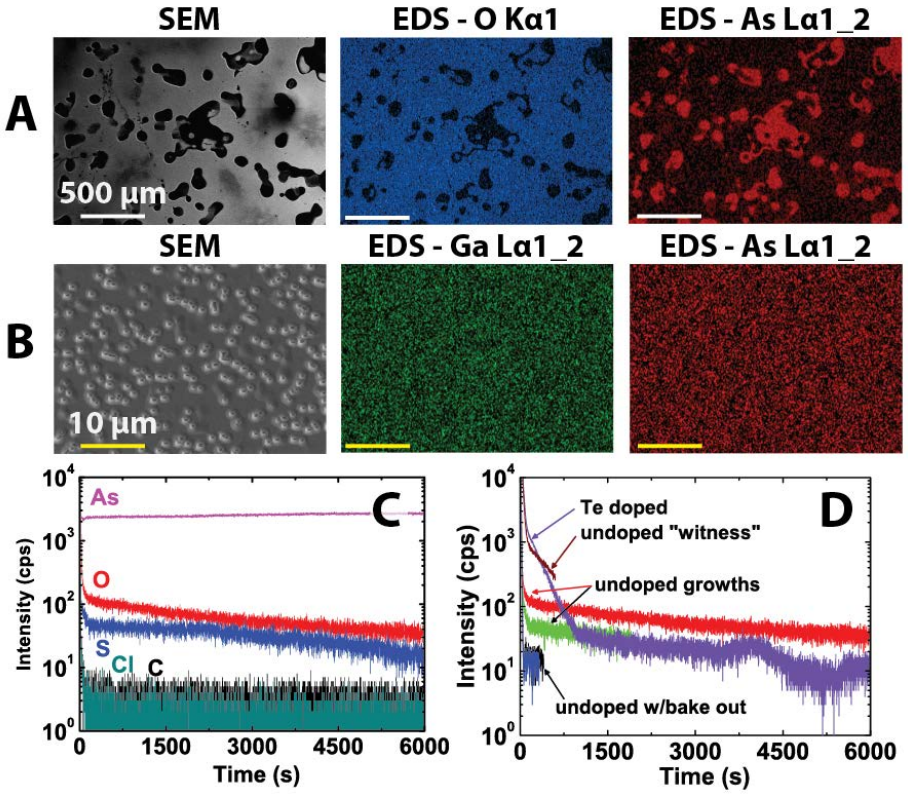

Figure 4: Investigation into oxygen content in both undoped and doped films. (a) SEM and EDS images of initial film grown by Cl-CSVT. Oxide present on surface. (b) SEM and EDS of pitted film. Surface is homogenous GaAs. (c) TOF-SIMS of undoped sample with oxygen and sulfur counts above background levels. (d) TOF-SIMS oxygen counts for a collection of films. Most recent films with bake outs prior to growth show reduced oxygen content.

mass spectrometry (TOF-SIMS) indicate there is still oxygen incorporation in our epitaxial films (Figure 4C). Subsequent heat treatment and vacuum pumping on these components

appears to have reduced any contaminants that were previously outgassing to an acceptable level at this time (Figure 4D).

In our TOF-SIMS measurements, there was also a sulfur signal similar to oxygen. Sulfur had previously been found in films grown in the H_2O-CSVT system (Figure 5A).[39] The graphite heaters were identified as the sulfur source then, and our graphite carriers were identified as the source here since the prototype carriers were made of machined, porous graphite. Hall effect measurements on those films with unintentional sulfur incorporation showed mobilities between 1050-1500 $cm^2\ V^{-1}\ s^{-1}$, corresponding to a donor concentration, N_D, of 1.1 ± 0.3 x 10^{19} cm^{-3}. This was consistent with the sulfur concentration of ~8 x 10^{18} cm^{-3} estimated from SIMS. TOF-SIMS measurements on films grown with pyrolytic graphite coated carriers did not show the same sulfur signal (Figure 5B). Continued use of pyrolytic coated graphite should sustain minimal sulfur incorporation into any film growths. Evaluation of intentional doping, cross-contamination, and further discussion on Hall effect measurements is contained in the subsequent section.

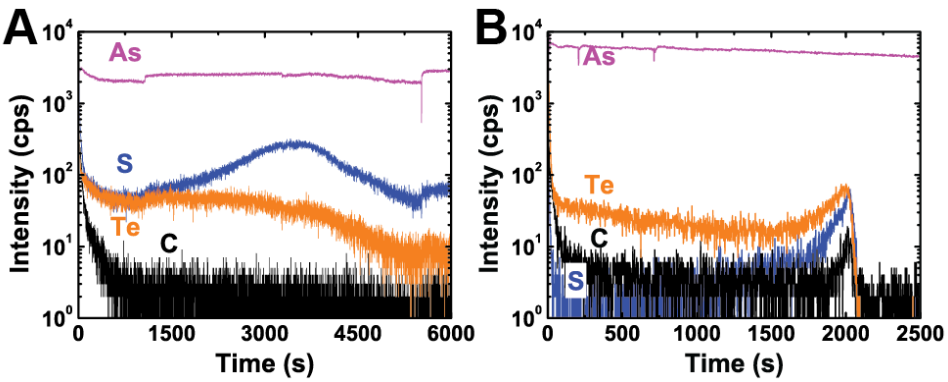

Figure 5: Investigation into sulfur content and effect of graphite carrier. (a) Te doped film using a porous graphite carrier. Sulfur concentration is comparable to Te. (b) Te doped film using pyrolytic coated graphite. Te content is comparable to that in (a) and sulfur content is within background levels.

Intentional Doping

With reduced levels of oxygen and sulfur, along with reductions in unwanted surface features, we executed simultaneous doped and undoped film growth to evaluate whether any cross contamination would occur. Both films were characterized TOF-SIMS, and Hall effect. High resolution ω scans of films grown prior to use with the new graphite were epitaxial, aligned to the <100> GaAs surface (Figure 6A), and we expect the films analyzed by TOF-SIMS and Hall to be epitaxial as well. TOF-SIMS data illustrates the ability of this system to execute simultaneous growths with minimal cross-contamination (Figure 6B). The removal of sulfur (within background detection), with the use of pyrolytic graphite, enabled the determination of electron mobility and approximate Te concentration via Hall effect measurements. We initially used Te as our dopant since it was found to transport with near unity efficiency in our H_2O-CSVT. A source wafer with dopant concentration of 1.96x10^{18} ± 0.32 cm^{-3} was used. Hall effect measurements determined the doped film had a carrier concentration of 4.07x10^{18} ± 1.42x10^{18} cm^{-3}, indicating near unity utilization of Te in this system as well (Figure 6C). The intentionally

undoped film had the highest mobility of 2156 $cm^2\ V^{-1}\ s^{-1}$. While there is limited data for the Cl-CSVT system, in comparison with the H_2O-CSVT data, these results indicate that Cl-CSVT from GaAs sources is competitive with MOVPE in terms of the achievable μ_e. Further details on doping and characterization can be found in the primary publication resulting from this work.[5]

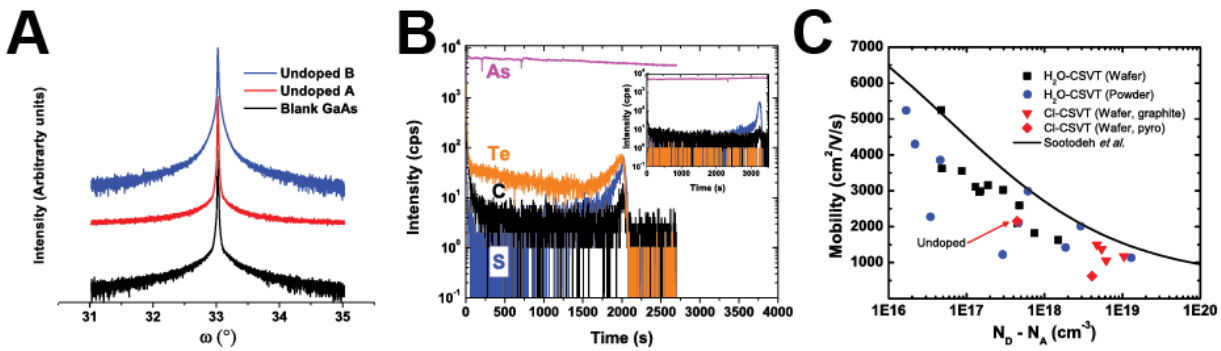

Figure 6: Characterization of *n*-type and undoped films. (a) XRD rocking curves show films grown by Cl-CSVT are single crystalline. (b) TOF-SIMS for Te doped film. Inset shows the same for the adjacently grown, intentionally undoped film. The absence of Te in the undoped film indicates there is little cross-contamination between adjacent growths. (c) Hall effect data of doped growth against historical H_2O-CSVT growths with MOVPE reference curve. Data for both types of graphite carrier are shown.

Film Morphologies:

Pitting and Hillocks

Despite reaching the growth rate target, all films exhibit unwanted surface features, including pits and non-planar growth (Figure 7). The pitting was initially thought to be caused by HCl etching during or after growth. The direct cause of the non-planar morphology (referred to as “hillocks” here) is still unknown but may be influenced by an orientation dependent growth mode discussed later. Under certain growth conditions, pits or hillocks have been eliminated (or reduced) but not both. Pitting was eliminated for growths at substrate temperatures below 700 °C by allowing the source and substrate to remain close-spaced while the system was evacuated and cooled below 100 °C (Figure 7B). The same was not true for the hillocks. These features can be on the order of 0.6 µm high and hundreds of microns wide (Figure 7D). At source temperatures closer to 800 °C, pitting was observed, despite the same cooling procedure and hillocks were still present. The ability to control either of these features is believed to be driven by either the growth temperatures, or the temperature ramp rate to or from growth setpoints, and the presence of HCl before or after growth. To further investigate the origin of the hillock feature we executed only the temperature ramp itself, stopping before growth of a film. Optical profilometry of these samples showed the early stage formation of these features for samples ramped under H_2 only and under 3000 ppm HCl-in-H_2 atmosphere (Figure 7C). At this time, the process conditions necessary to control pitting are more well understood than the hillocks. Further details on hillocks are provided in the following section investigating substrate orientation. Besides this, further investigation beyond the scope of this project will be needed to understand the origin of hillocks in more detail so as to control their formation.

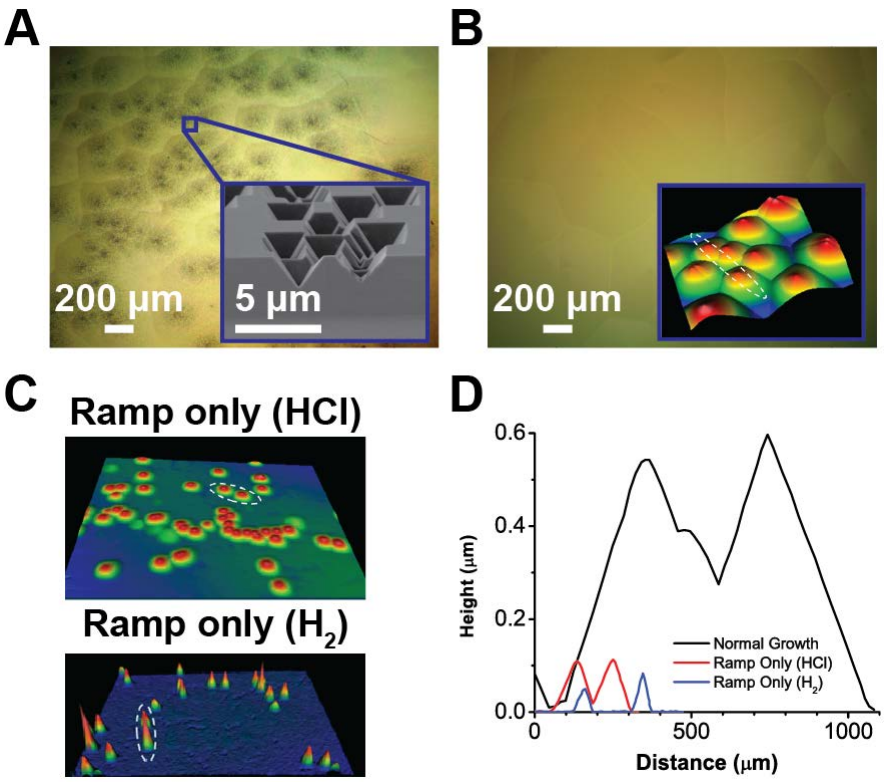

Figure 7: Surface features generated during growth. (a) Pitting on surface (SEM inset). These can be eliminated as seen in (b) but there is still a surface morphology. Optical profilometer inset shows general 3D features. (c) Optical profilometry images of films that only underwent the temperature ramp to growth temperature but no sustained growth. (d) Height profiles from profilometry line scan for corresponding films in (b) and (c).

Growth on Other Orientations

In addition to the apparent nucleation of these hillocks, orientation dependence of film growth, and any subsequent morphology, was also explored to gain further insight. Growth conditions for successful epitaxial growth on (100) GaAs were repeated for both (111)B and (111)A GaAs. Microscope and SEM images of these are shown in Figure 8. No growth was observed on (111)B GaAs, while small features were observed on (111)A GaAs (Figure 8B). The pits seen in multiple (100) samples (Figure 7A) are all terminated on (111) planes. In general, this suggests that the (111) plane is very stable under these growth conditions. This could have implications for selective area epitaxy if the growth rates of different orientations can be sufficiently controlled with growth temperature. Similar demonstrations have been made in MOVPE,[40] HVPE,[41] MBE,[42] and H_2O-CSVT.[20]

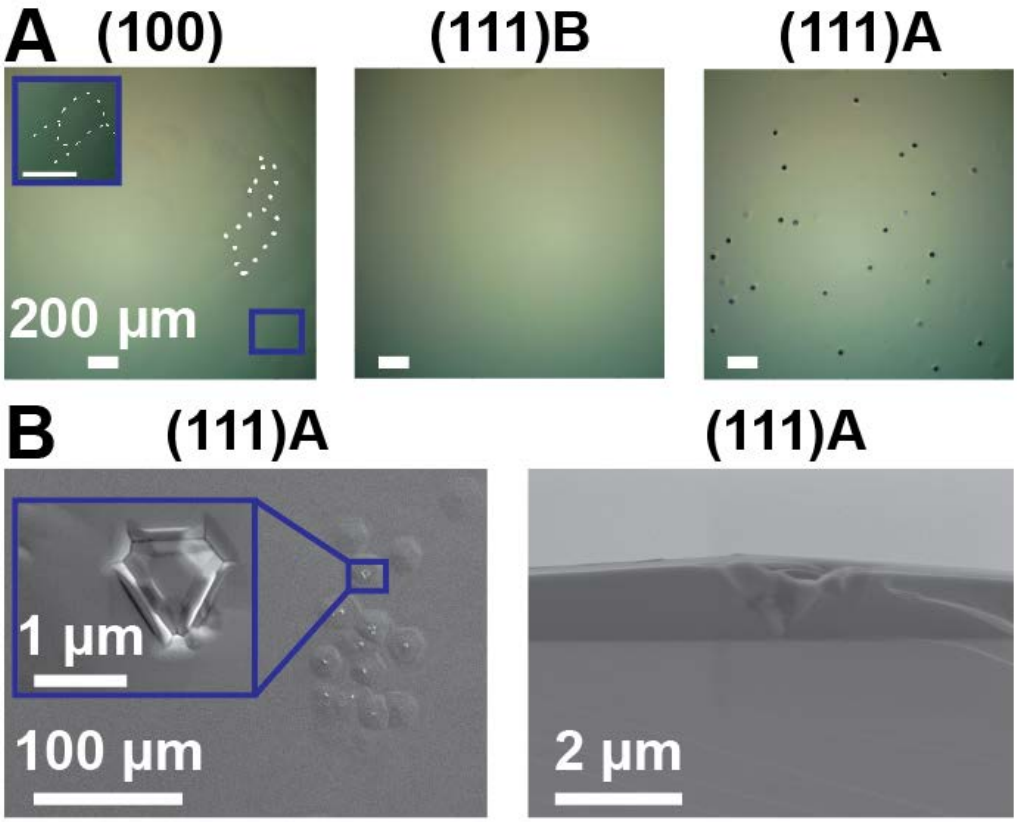

Figure 8: Growth dependence on substrate orientation. (a) Microscope images of wafer surface. (100) substrate has film growth and morphology. Morphology boundaries highlighted in inset and by dotted lines. (111)B substrate had no film growth. (111)A substrate had non-uniform growth features. These appear to be screw dislocations, as seen in (b) SEM images of (111)A surface and cross-section.

Growth on Si

The same growth conditions used for growths on different GaAs orientations were also tested on a (100) Si substrate. SEM imaging revealed the presence of small crystallites on the substrate (Figure 9). EDS mapping confirmed these crystallites were GaAs. These preliminary results indicate that direct deposition of GaAs on Si in the Cl-CSVT is possible and may be further improved under other growth conditions. This is also supported by the Au-catalyzed growth we were able to execute, highlighted in the following section.

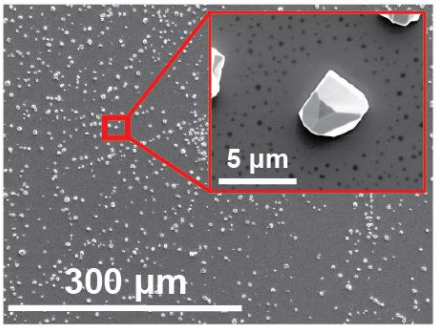

Figure 9: SEM images of GaAs growth on (100) Si substrate. Non-uniform nucleation of small GaAs crystallites was seen throughout the growth region. EDS confirmed crystallites were GaAs.

Au-catalyzed Growth

With the strong orientation dependent growth observed earlier we attempted a Au-catalyzed growth of GaAs nanowires. Ga- or Au-catalyzed growth has been demonstrated in other growth systems such as HVPE[17] and MBE[18,19] respectively but not in any CSVT system. To demonstrate proof of principle, ~2 nm of Au was deposited by evaporation onto each of the substrates already investigated and growth conditions were repeated. In contrast to the limited growth on any substrate besides (100) GaAs, significant growth features were observed on all films with the Au layer. SEM and optical profilometry images of these are shown in Figure 10.

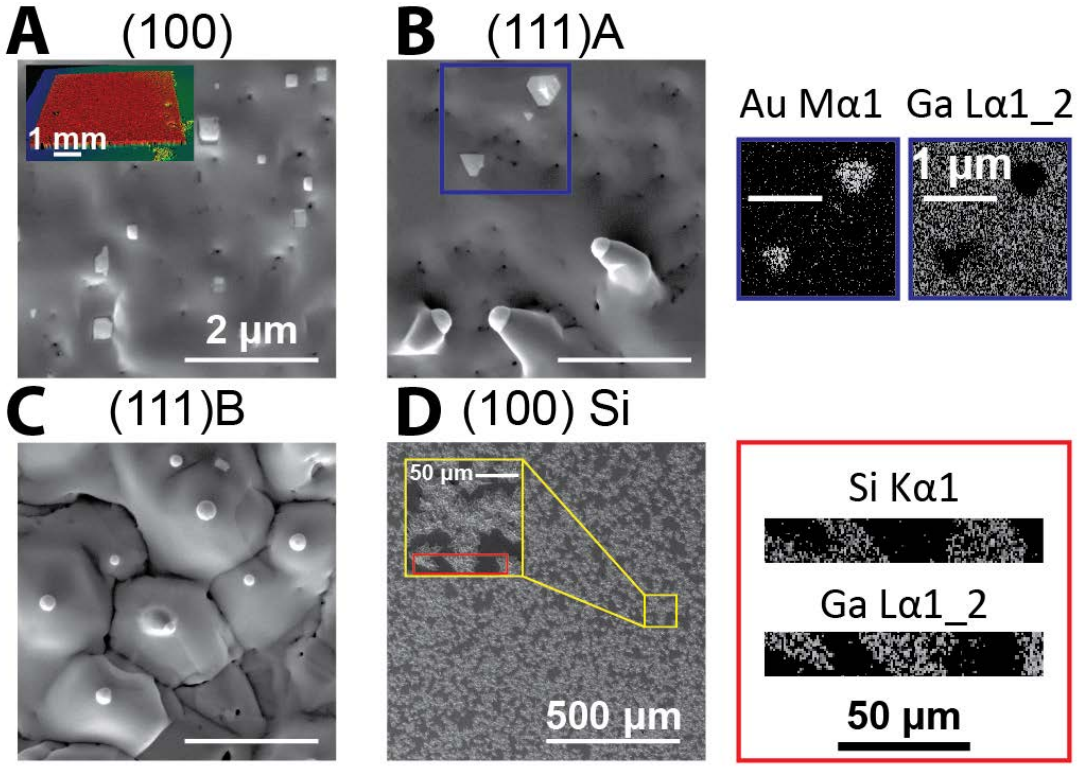

Figure 10: SEM plan view images of Au-catalyzed growth on GaAs and Si substrates. (a) No individual nanowire growth observed on (100) GaAs. Inset shows optical profilometry image of Au deposited region after growth. (b) Some nanowire formation on (111)A GaAs. EDS images for inset region, highlighting regions with Au on surface. (c) Hillocks with Au peaks seen on (111)B GaAs. (d) Polycrystalline GaAs growths on (100) Si substrate. EDS images of area highlighted in inset confirm GaAs growth and bare Si regions.

Conclusions:

We have demonstrated significant progress in understanding the conditions necessary for several types of growth. This includes:

- Successful *n*-type growth of homoepitaxial GaAs. The electronic characteristics of these materials grown by Cl-CSVT are nearly equivalent to MOVPE and H_2O-CSVT. There is minimal cross contamination between adjacent substrates, which will enable multiple growth experiments under the same process conditions using our four pocket graphite carriers.

- Initial investigations into selective area epitaxy and growth on Si with and without Au-catalyzed growth. Preliminary results indicate that Au-catalyzed growth can be used for selective growth on multiple substrate orientations. We also demonstrated growth on (100) Si substrates, which is promising for future work integrating a GaAs top cell on Si.

There were challenges in establishing the process conditions necessary for these accomplishments. This impacted our ability to execute the final two milestones of the project. However, the Cl-CSVT system works as intended and will enable to pursuit of those milestones beyond the bounds of this project. With these innovations, the team will be able to tackle the development of high-performance III-V single junctions and tandem devices directly on Si substrates in project phases subsequent to the 12-month SIPS program.

Budget and Schedule:

The table below shows the project spend plan on a per quarter basis. The planned and actual spending were similar.

Year	Quarter	From	To	A. Federal Share Initial Plan totals $225,000	B. Federal Share Updated Actuals & Plan	Cumulative Federal Share	C. Recipient Share Initial Plan totals $46,846	D. Recipient Share Updated Actuals & Plan	Cumulative Recipient Share
2016	Q3	7/1/2016	9/30/2016	$6,758.98	$6,774.93	$6,774.93	$0.00	$0.00	$0.00
2016	Q4	10/1/2016	12/31/2016	$100,000.00	$370.95	$7,145.88	$18,250.00	$0.00	$0.00
2017	Q1	1/1/2017	3/31/2017	$50,000.00	$16,546.33	$23,692.21	$18,250.00	$15,377.00	$15,377.00
2017	Q2	4/1/2017	6/30/2017	$40,000.00	$173,260.28	$196,952.49	$10,000.00	$41,109.00	$56,486.00
2017	Q3	7/1/2017	9/30/2017	$28,241.02	$28,047.51	$225,000.00	$9,986.00	$0.00	$56,486.00
Totals				**$225,000.00**	**$225,000.00**	$225,000.00	**$56,486.00**	**$56,486.00**	$56,486.00

The next table shows the spending category breakdown for expenses budgeted versus actual. Most categories are similar to that budgeted, with the exception of the equipment category. As reported to DOE in earlier quarterly reports, this was due to the additional purchase of a dry vacuum pump. Portions of the budget in other areas were used to support some of that additional cost.

Budget Categories per SF-424a	Approved Budget per SF-424A	Actual Expenses	
		This Reporting period (2017Q3)	Cumulative
a. Personnel	26,814.00	$3,238	$17,146
b. Fringe Benefits	9,439.00	$931	$7,917
c. Travel	-		
d. Equipment	-	$9,331	$12,272
e. Supplies	2,218.00	$1,545	$5,015
f. Contractual	200,735.00	$183,949	$183,949
g. Construction	-		
h. Other	5,624.00	$1,599	$2,399
i. Total Direct Charges	**$244,830**	**$200,593**	**$228,698**
j. Indirect Charges	37,016.00	$13,776	$24,740
k. Total Charges	**$281,846**	**$214,369**	**$253,438**
DOE Share	225,000.00	$173,260	$196,952
Cost Share	56,486.00	$41,109	$56,486
Cost Share Percentage	20.0%	19.2%	22.3%

Path Forward:

As previously addressed, the final tasks and milestones of the proposed project were unable to be attempted. Those centered around the growth of $Al_xGa_{1-x}As$ as a passivation layer. This, in addition to further tests of GaAs growth on Si, will serve as the next step in demonstrating more complete device geometries via CSVT than have been completed by our research group or others. As part of that, we will need to continue exploring the range of growth parameters for this system to execute these different growths. It has been previously demonstrated for the H_2O-CSVT system that temperature and water vapor concentration play a critical role in the growth process.[25,43] There is little information on how these parameters influence the growth of GaAs, or similar III-V semiconductors, and their corresponding electrical properties in Cl-CSVT. Future research will include a series of experiments varying the HCl concentration at different source temperatures. In doing so, we expect to vary the chemical equilibrium, and resultant concentration gradient, between gas species at the source and substrate. Since this gradient drives the diffusion limited growth, we may be able to control which gas species diffusion limits the growth. This may enable another way to control growth and provide conditions for planar growths with minimal surface defects as has been demonstrated in the H_2O-CSVT system.

The collective innovations of our Cl-CSVT system may ultimately serve as an enabling process for commercialization of the technology through a collaboration with appropriate industrial partners. This Cl-CSVT process is covered within the scope of a prior patent Boettcher et al. have based on the CSVT system (US Patent 9,368,670 B2).[44] Malachite Technologies Inc. is waiting to pursue possible commercialization of this system until additional results can sufficiently demonstrate both repeatable material and device quality and scalability.

Accomplishments:

Students Supported

C. J. Funch was supported part time by the DOE SIPS award. Other researchers who contributed to this work (graduate student A. L. Greenaway and postgraduate researcher J. W. Boucher) were both supported by other mechanisms during their work at the University of Oregon on this project.

Publications Resulting from This Work

(1) Greenaway, A. L.; Boucher, J. W.; Oener, S. Z.; Funch, C. J.; Boettcher, S. W. Low-Cost Approaches to III–V Semiconductor Growth for Photovoltaic Applications. *ACS Energy Lett.* **2017**, 2270–2282.

(2) Funch, C. J.; Greenaway, A. L.; Boucher, J. W.; Weiss, R.; Welsh, A.; Aloni, S.; Boettcher, S. W. A Close-Spaced Vapor Transport Reactor for III-V Growth Using HCl as the Transport Agent. *J. Cryst. Growth*. *In Preparation,* **2018**.

Acknowledgment: This material is based upon work supported by the Department of Energy, Office of Energy Efficiency and Renewable Energy (EERE), under Award Number DE-EE0007361.

References:

(1) Swanson, R. M. Approaching the 29% Limit Efficiency of Silicon Solar Cells. In *Conference Record of the Thirty-first IEEE Photovoltaic Specialists Conference, 2005.*; IEEE, 1961; pp 889–894.

(2) Green, M. A.; Hishikawa, Y.; Warta, W.; Dunlop, E. D.; Levi, D. H.; Hohl-Ebinger, J.; Ho-Baillie, A. W. H. Solar Cell Efficiency Tables (Version 50). *Prog. Photovoltaics Res. Appl.* **2017**, *25* (7), 668–676.

(3) Fthenakis, V. M.; Bowerman, B. Environmental Health and Safety (EHS) Issues in III-V Solar Cell Manufacturing. *3rd World Conf. onPhotovoltaic Energy Conversion, 2003. Proc.* **2003**, *1*, 1–4.

(4) Greenaway, A. L.; Boucher, J. W.; Oener, S. Z.; Funch, C. J.; Boettcher, S. W. Low-Cost Approaches to III–V Semiconductor Growth for Photovoltaic Applications. *ACS Energy Lett.* **2017**, *2* (10), 2270–2282.

(5) Funch, C. J.; Greenaway, A. L.; Boucher, J. W.; Weiss, R.; Welsh, A.; Aloni, S.; Boettcher, S. W. A Close-Spaced Vapor Transport Reactor for III-V Growth Using HCl as the Transport Agent. *J. Cryst. Growth* **2018**, *In Preparation.*

(6) Murali, K. R.; Jayachandran, M.; Rangarajan, N. Review of Techniques on Growth of GaAs and Related Compounds. *Bull. Electrochem. Mater. Sci.* **1987**, *3* (3), 261–265.

(7) Rahman, M. M.; Hasan, N. M. Compound Semiconductor Epitaxial Growth Techniques. *Int. J. thin Film. Sci. techology* **2016**, *5* (1), 45–49.

(8) Bobela, D. C.; Gedvilas, L.; Woodhouse, M.; Horowitz, K. A. W.; Basore, P. A. Economic Competitiveness of III-V on Silicon Tandem One-Sun Photovoltaic Solar Modules in Favorable Future Scenarios. *Prog. Photovoltaics Res. Appl.* **2017**, *25* (1), 41–48.

(9) Biefeld, R. M.; Koleske, D. D.; Cederberg, J. G. *The Science and Practice of Metal-Organic Vapor Phase Epitaxy (MOVPE)*, Second Edi.; Elsevier B.V., 2015.

(10) Holloway, P. H.; McGuire, G. E. *Handbook of Compound Semiconductors*; 1995.

(11) Schulte, K. L.; Rance, W. L.; Reedy, R. C.; Ptak, A. J.; Young, D. L.; Kuech, T. F. Controlled Formation of GaAs Pn Junctions during Hydride Vapor Phase Epitaxy of GaAs. *J. Cryst. Growth* **2012**, *352* (1), 253–257.

(12) Simon, J.; Young, D.; Ptak, A. Low-Cost III-V Solar Cells Grown by Hydride Vapor-Phase Epitaxy. In *2014 IEEE 40th Photovoltaic Specialist Conference (PVSC)*; IEEE, 2014; pp 0538–0541.

(13) Simon, J.; Schulte, K. L.; Jain, N.; Johnston, S.; Young, M.; Young, M. R.; Young, D. L.; Ptak, A. J. Upright and Inverted Single-Junction GaAs Solar Cells Grown by Hydride Vapor Phase Epitaxy. *IEEE J. Photovoltaics* **2017**, *7* (1), 157–161.

(14) Jain, N.; Simon, J.; Schulte, K. L.; Dippo, P.; Young, M.; Young, D. L.; Ptak, A. J. InGaAsP Solar Cells Grown by Hydride Vapor Phase Epitaxy. In *2016 IEEE 43rd Photovoltaic Specialists Conference (PVSC)*; Portland, OR, 2016; pp 1090–1094.

(15) Zheng, M.; Wang, H.-P.; Sutter-Fella, C. M.; Battaglia, C.; Aloni, S.; Wang, X.; Moore, J.; Beeman, J. W.; Hettick, M.; Amani, M.; et al. Thin-Film Solar Cells with InP Absorber Layers Directly Grown on Nonepitaxial Metal Substrates. *Adv. Energy Mater.* **2015**, *5* (22), 1501337.

(16) Chen, K.; Kapadia, R.; Harker, A.; Desai, S.; Seuk Kang, J.; Chuang, S.; Tosun, M.; Sutter-Fella, C. M.; Tsang, M.; Zeng, Y.; et al. Direct Growth of Single-Crystalline III-V Semiconductors on Amorphous Substrates. *Nat. Commun.* **2016**, *7*, 1–6.

(17) Dong, Z.; André, Y.; Dubrovskii, V. G.; Bougerol, C.; Leroux, C.; Ramdani, M. R.; Monier, G.; Trassoudaine, A.; Castelluci, D.; Gil, E. Self-Catalyzed GaAs Nanowires on Silicon by Hydride Vapor Phase Epitaxy. *Nanotechnology* **2017**, *28*

(12), 125602.

(18) Wu, Z. H.; Mei, X. Y.; Kim, D.; Blumin, M.; Ruda, H. E. Growth of Au-Catalyzed Ordered GaAs Nanowire Arrays by Molecular-Beam Epitaxy. *Appl. Phys. Lett.* **2002**, *81* (27), 5177–5179.

(19) Harmand, J. C.; Patriarche, G.; Péré-Laperne, N.; Mérat-Combes, M.-N.; Travers, L.; Glas, F. Analysis of Vapor-Liquid-Solid Mechanism in Au-Assisted GaAs Nanowire Growth. *Appl. Phys. Lett.* **2005**, *87* (20), 203101.

(20) Greenaway, A. L.; Sharps, M. C.; Boucher, J. W.; Strange, L. E.; Kast, M. G.; Aloni, S.; Boettcher, S. W. Selective Area Epitaxy of GaAs Microstructures by Close-Spaced Vapor Transport for Solar Energy Conversion Applications. *ACS Energy Lett.* **2016**, *1* (2), 402–408.

(21) Cattoni, A.; Scaccabarozzi, A.; Chen, H.-L.; Oehler, F.; Himwas, C.; Patriarche, G.; Tchernycheva, M.; Harmand, J.-C.; Collin, S. III-V Nanowires on Silicon: A Possible Route to Si-Based Tandem Solar Cells. In *Light, Energy and the Environment*; OSA: Washington, D.C., 2017; Vol. Part F71-P, p PM3A.2.

(22) Nicoll, F. H. The Use of Close Spacing in Chemical-Transport Systems for Growing Epitaxial Layers of Semiconductors. *J. Electrochem. Soc.* **1963**, *110* (11), 1165.

(23) Perrier, G.; Philippe, R.; Dodelet, J. P. Growth of Semiconductors by the Close-Spaced Vapor Transport Technique: A Review. *J. Mater. Res.* **1988**, *3* (5), 1031–1042.

(24) Ladd, G. O.; Feucht, D. L. Autodoping Effects at the Interface of GaAs-Ge Heterojunctions. *Metall. Mater. Trans. B* **1970**, *1* (3), 609–616.

(25) Ritenour, A. J.; Cramer, R. C.; Levinrad, S.; Boettcher, S. W. Efficient *N*-GaAs Photoelectrodes Grown by Close-Spaced Vapor Transport from a Solid Source. *ACS Appl. Mater. Interfaces* **2012**, *4* (1), 69–73.

(26) Deschler, M.; Cüppers, M.; Brauers, A.; Heyen, M.; Balk, P. Halogen VPE of AlGaAs for Optoelectronic Device Applications. *J. Cryst. Growth* **1987**, *82* (4), 628–638.

(27) Heyen, M.; Balk, P. Epitaxial Growth of GaAs in Chloride Transport Systems. *Prog. Cryst. Growth Charact.* **1983**, *6* (3), 265–303.

(28) Le Bel, C.; Cossement, D.; Dodelet, J. P.; Leonelli, R.; DePuydt, Y.; Bertrand, P. Doping and Residual Impurities in GaAs Layers Grown by Close-spaced Vapor Transport. *J. Appl. Phys.* **1993**, *73* (3), 1288–1296.

(29) Weiner, M. E. Si Contamination in Open Flow Quartz Systems for the Growth of GaAs and GaP. *J. Electrochem. Soc.* **1972**, *119* (4), 496.

(30) Briggs, A. T. R.; Butler, B. R. A Study of Residual Background Doping in High Purity Indium Phosphide Grown by Atmospheric Pressure OMVPE. *J. Cryst. Growth* **1987**, *85* (3), 535–542.

(31) Chung, D. D. L. Review Graphite. *J. Mater. Sci.* **2002**, *37* (8), 1475–1489.

(32) Hennig, G. The Properties of the Interstitial Compounds of Graphite. III. The Electrical Properties of the Halogen Compounds of Graphite. *J. Chem. Phys.* **1952**, *20* (9), 1443–1447.

(33) Garverick, L. Corrosion by Hydrogen Chloride and Hydrochloric Acid. In *Corrosion in the Petrochemical Industry*; 1994; pp 191–197, 423–425.

(34) Schillmoller, C. M. *Alloys to Resist Chlorine, Hydrogen Chloride and Hydrochloric Acid*; 1988.

(35) Ma, F.-Y. Chapter 7: Corrosive Effects of Chlorides on Metals. In *Pitting Corrosion*; 2012; pp 139–178.

(36) Nickel Development Institute. *Design Guidelines for the Selection and Use of Stainless Steel*.

(37) Windhorst, T.; Blount, G. Carbon-Carbon Composites: A Summary of Recent Developments and Applications. *Mater. Des.* **1997**, *18* (1), 11–15.

(38) Côté, D.; Dodelet, J. P.; Lombos, B. A.; Dickson, J. I. Epitaxy of GaAs by the Close-Spaced Vapor Transport Technique. *J. Electrochem. Soc.* **1986**, *133* (9), 1925–1934.

(39) Boucher, J. W.; Ritenour, A. J.; Greenaway, A. L.; Aloni, S.; Boettcher, S. W. Homojunction GaAs Solar Cells Grown by Close Space Vapor Transport. In *2014 IEEE 40th Photovoltaic Specialist Conference (PVSC)*; IEEE, 2014; pp 0460–0464.

(40) Lebens, J. A.; Tsai, C. S.; Vahala, K. J.; Kuech, T. F. Application of Selective Epitaxy to Fabrication of Nanometer Scale Wire and Dot Structures. *Appl. Phys. Lett.* **1990**, *56* (26), 2642–2644.

(41) Gil-Lafon, E.; Napierala, J.; Castelluci, D.; Pimpinelli, A.; Cadoret, R.; Gérard, B. Selective Growth of GaAs by HVPE: Keys for Accurate Control of the Growth Morphologies. *J. Cryst. Growth* **2001**, *222* (3), 482–496.

(42) Lee, S.-C.; Malloy, K. J.; Brueck, S. R. J. Nanoscale Selective Growth of GaAs by Molecular Beam Epitaxy. *J. Appl. Phys.* **2001**, *90* (8), 4163–4168.

(43) Boucher, J.; Boettcher, S. Arsenic Antisite and Oxygen Incorporation Trends in GaAs Grown by Water-Mediated Close-Spaced Vapor Transport. *J. Appl. Phys.* **2017**, *121* (9), 93102.

(44) Boettcher, S. W.; Ritenour, A. J.; Boucher, J. W.; Greenaway, A. L. GaAs Thin Films and Methods of Making and Using the Same. U.S. Patent 9,368,670 B2, 2016.